NANOPHOTONICS

Remote structuring of near-field landscapes

Vincent Ginis[1,2]*, Marco Piccardo[1,3], Michele Tamagnone[1], Jinsheng Lu[1,4], Min Qiu[5], Simon Kheifets[1], Federico Capasso[1]*

The electromagnetic near field enables subwavelength applications such as near-field microscopy and nanoparticle manipulation. Present methods to structure the near field rely on optical antenna theory, involving nanostructures that locally convert propagating waves into confined near-field patterns. We developed a theory of remote rather than local near-field shaping, based on cascaded mode conversion and interference of counterpropagating guided waves with different propagation constants. We demonstrate how to structure at will the longitudinal and transverse variation of the near field, allowing for distributions beyond the conventional monotonic decay of the evanescent field. We provide an experimental realization that confirms our theory. Our method applies to fields with arbitrary polarization states and mode profiles, providing a path toward three-dimensional control of the near field.

Guided modes are solutions of Maxwell's equations in which the energy of the field is propagating exclusively inside a confining structure, known as a waveguide. In the region surrounding the waveguide, there is typically a non-negligible field: the near field of confined modes (*1*). One of the main reasons for increased interest in the near field is the very high resolution that can be obtained with near-field imaging (*2*). This has led to the development of near-field scanning optical microscopes (*3*). Other applications include near-field sensing (*4*), nonradiative energy transfer (*5*), and the use of near-field optical forces to manipulate particles (*6*). Recently, it was shown that the near field can exert a counterintuitive force on a microparticle (*7*, *8*). Tunneling of light between coupled waveguides is another near-field phenomenon that is particularly useful in the context of interferometry, quantum optics, optical computing, and telecommunications (*9*–*12*).

Several techniques have emerged to structure this field (*13*–*15*). These techniques predominantly use a perspective based on classical antenna theory, where dielectric or plasmonic scatterers convert propagating waves into localized near-field radiation patterns (*16*, *17*). In sharp contrast, the design techniques of far-field radiation patterns rely on Fourier optics (*18*). These methods are based on the interference of waves with different spatial frequencies and often use simple geometric principles, known as Fermat's principle, holography, conformal mapping, or transformation optics (*19*–*21*).

The idea behind our technique is the structuring of the near field based on the interference of many counter propagating guided waves with different propagation constants. We use β to refer to the longitudinal component of the guided-mode wave vector ($\beta = k_0 n_{\mathrm{eff}}$, where k_0 is the free-space wave vector and n_{eff} is the effective mode index). The region of interest, which we call the arena, is delineated by two mode converters (Fig. 1D). One guided mode enters the arena on one side and interacts with the mode converter on the other side. This process generates a different counterpropagating mode, which in turn interacts with the leftmost mode converter. The cascaded interaction between the newly generated modes and the mode converters creates a sum of many guided waves (Fig. 1C). The physical properties of the converters entirely determine the phase and amplitude of the guided modes in the arena. We show that if the waveguide supports a sufficient number of modes, this process allows for the creation of a near-arbitrary near-field landscape above the arena. Because of the discrete nature of the confined modes and the specific spacing of the longitudinal wave vectors (Fig. 1A), it is possible to design reflectors that convert one particular mode into another while leaving the other modes virtually unaffected. Indeed, in reciprocal space, a mode converter can be pictured as imparting a vector that matches the difference between the propagation constants of two counterpropagating modes of interest (Fig. 1B).

We illustrate the mechanism for a three-mode waveguide with incoming mode β_3 in Fig. 1, E to G. The principle can be generalized to configurations with other incident modes and systems with more than three modes using gratings with different periodicities (*22*). While the amplitude of the near field oscillates at high frequencies, its envelope (or the intensity) remains constant as a function of time (Fig. 1G). The time-independent spatial variation of the near-field intensity is given by

$$\frac{I_{\mathrm{arena}}}{I_0} = \sum_{i=1}^{N}\left(\prod_{j=0}^{i-1} r_j^2\right) + 2\sum_{l=2}^{N}\sum_{m=1}^{l-1}\left\{\prod_{p=0}^{l-1} r_p \prod_{q=0}^{m-1} r_q \cos\left[(\beta_l - \beta_m)x - \sum_{r=m}^{l}\varphi_r\right]\right\} \quad (1)$$

where $\{r_j\}$ are the reflection coefficients of the mode converters, and $\{\phi_i\}$ and $\{\beta_i\}$ are respectively the phases and the longitudinal wave vectors of the modes propagating in the system, in the order in which the modes are generated. The reflection coefficients are determined both by the mode-conversion efficiency and by the differences between the field strengths of the different modes at the interface (*22*). Some counterintuitive properties arise because of the cascade mode conversion: the absence of a round-trip phase condition, the possibility of field enhancement over a large frequency range, and standing waves with time-varying nodes (*22*).

The second term in Eq. 1 has similarities to a Fourier series. However, the contributing frequencies that determine the spatial intensity profile are not equidistant, but rather are a set of difference frequencies ($\beta_i - \beta_j$). Nonetheless, our analysis shows that, similar to a standard Fourier series, many spatial profiles can be approximated arbitrarily well by the sum of cosines, shown in Eq. 1. We calculated the reflection coefficients—both amplitude and phase—that yield the best fit of a target landscape (*22*). In Fig. 2, A to C, we show the optimal decompositions of a sigmoid function, a bell curve, and a straight line, respectively.

These profiles are realized in the region above the waveguide. At distances farther away from the interface, the intensity will have decreased exponentially. The shape of the landscape will also have changed because of the different decay constants of the guided modes. However, it is possible to incorporate the different decay constants into the model and design the landscape at a specific distance away from the interface.

Just a few guided modes can generate a rich range of near-field profiles. Von Neumann said once: "With four parameters I can fit an elephant, and with five I can make him wiggle his trunk" (*23*). In Fig. 2D, we show that it is indeed possible to design a near-field landscape shaped like an elephant (*24*) using only four modes. This is possible because the periodicity of the signals, determined by Eq. 1, is greater than the length of the region where one wants to design a specific field distribution. In other words, by choosing a small arena length relative to the signal period, one can extract a small part of a more extended signal (Fig. 2D).

[1]Harvard John A. Paulson School of Engineering and Applied Sciences, Harvard University, Cambridge, MA 02138, USA. [2]Data Lab/Applied Physics, Vrije Universiteit Brussel, 1050 Brussels, Belgium. [3]Center for Nano Science and Technology, Istituto Italiano di Tecnologia, 20133 Milan, Italy. [4]State Key Laboratory of Modern Optical Instrumentation, College of Optical Science and Engineering, Zhejiang University, 310027 Hangzhou, China. [5]Key Laboratory of 3D Micro/Nano Fabrication and Characterization of Zhejiang Province, School of Engineering, Westlake University, Hangzhou 310024, China.
*Corresponding author. Email: ginis@seas.harvard.edu (V.G.); capasso@seas.harvard.edu (F.C.)

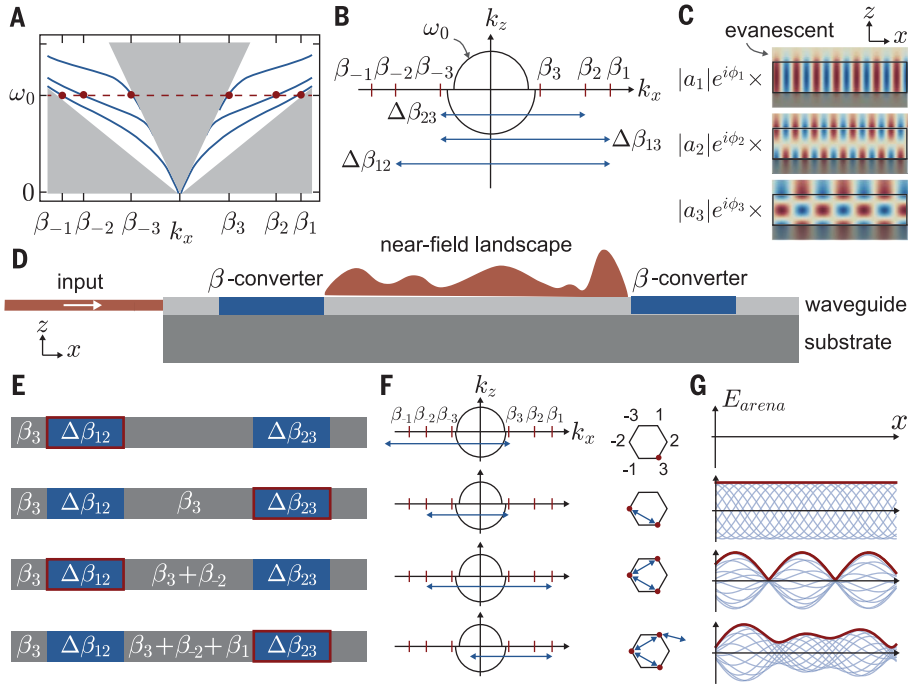

Fig. 1. Remote near-field engineering using β-converters. (**A**) The dispersion relation of a waveguide shows the discrete set of modes with in-plane propagation constants k_x that can exist (red dots) at a fixed frequency (red dashed line). (**B**) The modes at ω_0 visualized in the (k_x,k_z) plane, where the semicircles represent the dispersion relations of the surrounding media. In this reciprocal space, β-converters correspond to vectors that bridge the distance between a specific pair of counterpropagating modes with different mode indices. (**C**) By controlling independently the amplitude $|a_i|$ and phase ϕ_i of each of the guided modes, we can create near-field spatial profiles. We show the (x,z) cross section of the fundamental, the second, and the third guided mode. (**D**) A schematic of a near-field landscape device. A single mode at the input of a multimode waveguide iteratively interacts with two β-converters and generates a set of guided modes with different complex amplitudes, generating a near-field landscape. (**E** to **G**) Step-by-step round-trip mechanism in four consecutive steps (top to bottom). The interactions are visualized in physical space (E) and in reciprocal space (F). Also shown are compact diagrams representing the mode conversion as a path on a polygon where each vertex corresponds to a different guided mode. (G) The evanescent near field that is generated at the interface in the arena.

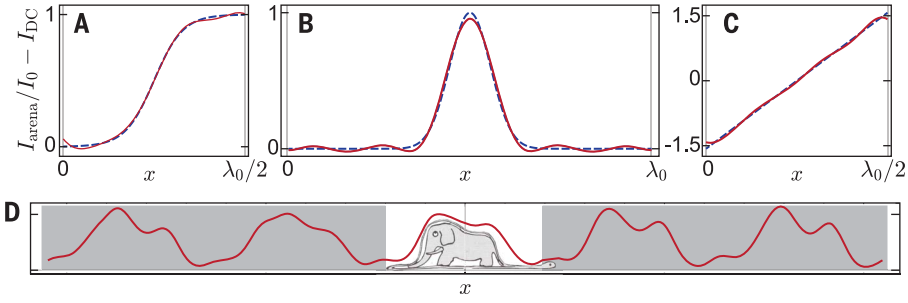

Fig. 2. Designing longitudinal landscapes. (**A** to **D**) With only a few free parameters, the near-field landscape can be fitted to a large class of predetermined functions (dashed lines), such as a sigmoid (A), a Gaussian (B), a straight line (C), and an elephant shape (*24*) (D). Each panel shows the spatial variation of the near-field intensity (I_{arena}/I_0) − I_{DC}, where I_{DC} is the first term in Eq. 1. All these examples are reconstructed in a four-mode system ($n_{eff,1}$ = 3.36, $n_{eff,2}$ = 2.6, $n_{eff,3}$ = 1.9, $n_{eff,4}$ = 1.1).

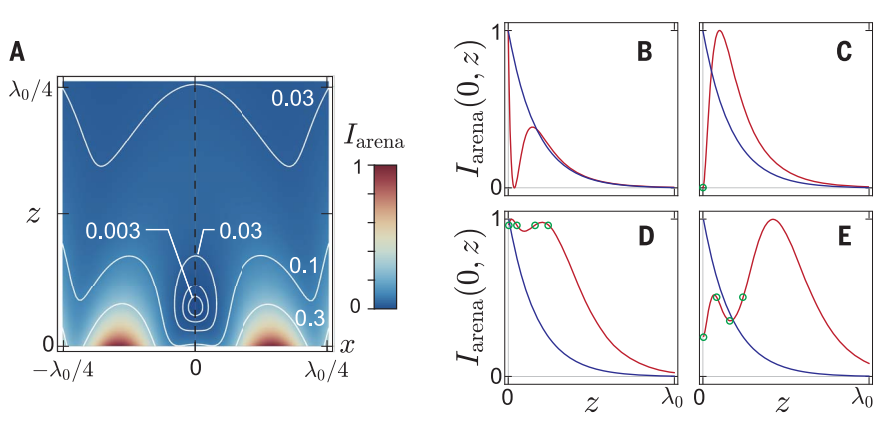

Fig. 3. Designing transverse landscapes. Transverse variations of the near-field intensity can be designed by interfering evanescent waves with different decay constants. (**A**) An (x,z) density plot of a specific near-field intensity illustrates a nonmonotonic decay of the near field in the transverse direction at x = 0. We construct an isolated intensity minimum above the interface. (**B**) A cross section of the field shown in (A) at x = 0 (dashed line), highlighting the transverse profile of the evanescent field (red). (**C** to **E**) Other structured, transverse near-field profiles exhibiting an intensity node at the interface (C), an intensity plateau (D), and an oscillatory intensity profile (E). The amplitudes of the modes are determined by an algorithm that fits the near-field intensity to target intensities, indicated by the green circles. In each of these plots, the structured fields are normalized at the interface, and the blue lines show the cross section of the fundamental mode. The structured near fields are calculated using a combination of the first five modes of a symmetric slab silicon-on-insulator waveguide (V number = 18).

Our theory has other possible uses beyond designing the field profile along the propagation direction. It can also be used to synthesize unusual transverse near-field profiles—that is, in the direction perpendicular to the interface. Modes with different propagation constants β_i have different decay constants $\gamma_i = (\beta_i^2 - k_0^2)^{1/2}$. As a result, it is possible to generate different interference patterns above the interface. One of the most intriguing consequences of this phenomenon is the fact that the intensity of the field does not have to be a monotonously descending function, starting from the interface. Under the right conditions, the interference of several evanescent fields may

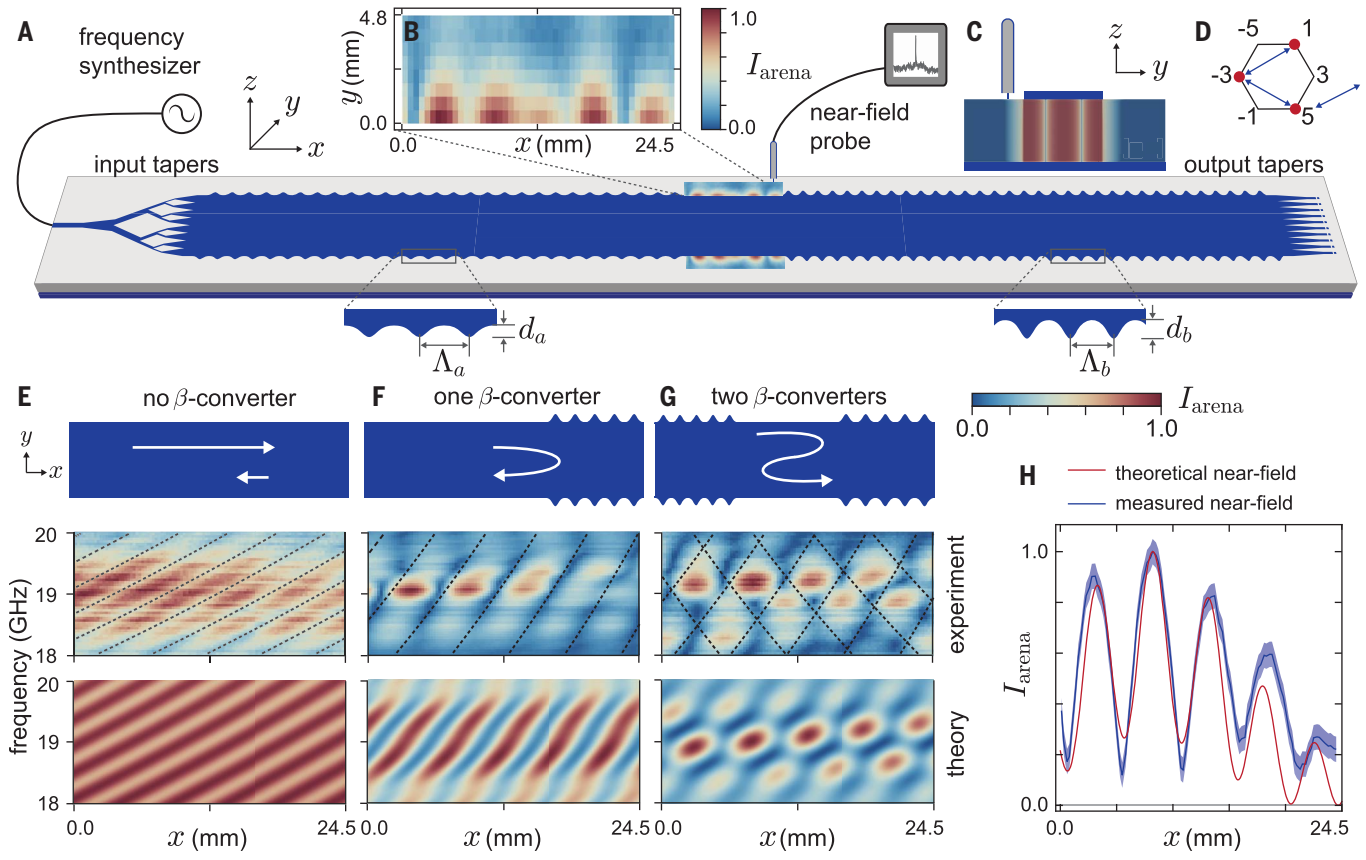

Fig. 4. Measurement of a near-field landscape. (**A**) Schematic of the device and characterization setup. A multimode microstrip is fed by a frequency synthesizer at 19 GHz. Two β-converters are fabricated by corrugation of the top copper layer. (**B**) Example of a measured near field. (**C**) Schematic cross section of the microstrip illustrating the geometry in which the probe measures the near field. A simulation of the third mode of the waveguide (β_3) is shown in a logarithmic scale. (**D**) Polygon diagram encoding the chained mode conversion. (**E** to **G**) Experimental and theoretical maps in the space-frequency domain of the near field of three devices: a bare microstrip without converters, one with a single β-converter, and one with a pair of β-converters. The near-field signal is characterized using a line scan on top of the dielectric in the longitudinal direction for a 2-GHz interval around the design frequency (f_0 = 19 GHz). From top to bottom: A schematic of the top metal layer; the experimental maps with superimposed analytical curves (dashed lines); the theoretical maps, obtained using a single-parameter fit. The checkered pattern observed in (G) is a space-frequency signature of a full round trip in the arena via double mode conversion. (**H**) Line cuts around f_0 of the experimental and theoretical maps for the device with two β-converters.

grow to a maximum before the field starts to descend (Fig. 3).

We implemented an algebraic technique that allows for the design of some nontrivial transverse landscapes (*22*). For a fixed x-coordinate, one can explicitly set the intensity at different heights to predetermined values $I(x, z)$. In Fig. 3B, we compare the intensity profile of a traditional evanescent wave with the intensity profile of a structured near field, with an intensity minimum at a small distance away from the interface. In Fig. 3, C to E, we display the profiles of several structured near fields, respectively corresponding to an intensity profile with a node at the interface (C), a plateau (D), and strong oscillatory variations (E).

Two subtle trade-offs appear. First, the more one wants to deviate from a traditional exponential decay, the smaller the region (in the x-direction) where one can obtain this variation. Second, in the region where substantial nonmonotonic changes are occurring, the intensity will increase only to a fraction of the total intensity in the system. Both trade-offs are shown in Fig. 3A. These two considerations have a lot in common with the trade-offs that are typically associated with superoscillating functions (*25*).

To experimentally demonstrate our theory, we realized a device that includes the key mechanisms presented above. We designed a near field that combines small feature sizes and large intensity variations that can be obtained with a three-mode system. The scale invariance of Maxwell's equations ensures that the technique applies to electromagnetic waves of any frequency. We carried out the experiment at microwave frequencies: The device consists of a multimode microstrip with an arena embedded into a pair of β-converters fabricated through a corrugation of the top metal layer (Fig. 4A) to ensure the chained mode conversion $\beta_1 \rightarrow \beta_{-3} \rightarrow \beta_5$ (Fig. 4D) at the design frequency f_0 = 19 GHz. The microstrip is fed by a microwave synthesizer and uses a collection of input tapers to inject the fundamental mode of the waveguide (β_1) as well as output tapers absorbing any transmitted mode (*22*).

The landscape was measured by near-field scanning microwave microscopy (Fig. 4, A and C). This technique uses a scanning probe placed near the sample to measure the surface field beyond the diffraction limit (*26*). Figure 4B shows a measured z-polarized near-field signal. In the x-direction, parallel to the mode propagation, multiple peaks with different intensities are observed, corresponding to the desired longitudinal landscape. In the perpendicular y-direction, the features decay away from the waveguide, as expected.

We study the evolution of a single line scan along the x-direction as a function of the injected frequency in a small interval around f_0.

We start with the simple device without converters (Fig. 4E). In this case, one observes at any frequency a periodic signal modulation in space, in agreement with a traditional standing wave, caused by the residual reflection at the output taper. The position of the interference nodes describes hyperbolic curves in the space-frequency domain. From their period we obtain the effective index of the propagating mode: 1.706 ± 0.036, in agreement with the theoretical value of the fundamental mode, 1.705.

Next, we examine the behavior of a device embedding one β-converter (Fig. 4F). Here again, a stripe pattern appears, but the period and the tilt of the hyperbolas have changed—a mode conversion signature (*22*). The pattern can be reproduced from theory by using only one fit parameter (ϕ_{13}).

Finally, we turn our attention to the device with two β-converters (Fig. 4G). In this case, a peculiar checkered pattern is observed. Despite its complexity, the origin of this pattern can be understood as due to the intertwining of two families of hyperbolas—each appearing because of the reflection at one of the mode converters—which defines tiles in the space-frequency domain filled with near-field hotspots. This checkered pattern is also obtained from theory (*22*), again using only one free parameter (ϕ_{35}). The agreement between experiments and theory is further highlighted by comparing a line cut of the space-frequency plots around f_0 (Fig. 4H). These results confirm that a full round trip via mode conversion in the arena is completed and a near-field landscape in agreement with the theory is created.

We introduced the concept of cascaded mode conversion to remotely control the near field at an interface. No antennas are present in the area of interest. As a result, there is substantial freedom in the design, which allows for instance for a nonmonotonic variation of the near field. Several free parameters can be added to enable the design of nontrivial polarization and vector near fields (*27*). Nanowaveguides with engineered mode indices or near-zero refractive indices could be useful to tune the overall bandwidth of the designed landscapes (*28*, *29*). Like many other methods in electromagnetism, our technique could find its way into the manipulation of different waves in physics (*30*).

REFERENCES AND NOTES

1. C. Girard, C. Joachim, C. Gauthier, *Rep. Prog. Phys.* **63**, 893–938 (2000).
2. L. Novotny, *Prog. Opt.* **50**, 137–184 (2007).
3. E. A. Ash, G. Nicholls, *Nature* **237**, 510–512 (1972).
4. L. Novotny, B. Hecht, *Principles of Nano-optics* (Cambridge Univ. Press, 2012).
5. P. Andrew, W. L. Barnes, *Science* **290**, 785–788 (2000).
6. M. Nieto-Vesperinas, P. Chaumet, A. Rahmani, *Philos. Trans. R. Soc. A* **362**, 719 (2004).
7. K. Y. Bliokh, A. Y. Bekshaev, F. Nori, *Nat. Commun.* **5**, 3300 (2014).
8. L. Liu *et al.*, *Phys. Rev. Lett.* **120**, 223901 (2018).
9. D. A. Miller, *Science* **347**, 1423–1424 (2015).
10. M. Tillmann *et al.*, *Nat. Photonics* **7**, 540–544 (2013).
11. J. Carolan *et al.*, *Science* **349**, 711–716 (2015).
12. S. Bogdanov, M. Shalaginov, A. Boltasseva, V. M. Shalaev, *Opt. Mater. Express* **7**, 111 (2017).
13. V. Fernández-Hurtado, F. J. García-Vidal, S. Fan, J. C. Cuevas, *Phys. Rev. Lett.* **118**, 203901 (2017).
14. S. Wei *et al.*, *Sci. Adv.* **4**, eaao0533 (2018).
15. S. Hu *et al.*, *Sci. Adv.* **4**, eaat2355 (2018).
16. D. Pohl, *Near-Field Optics: Principles and Applications* (World Scientific, 2000), pp. 9–21.
17. A. I. Kuznetsov, A. E. Miroshnichenko, M. L. Brongersma, Y. S. Kivshar, B. Luk'yanchuk, *Science* **354**, aag2472 (2016).
18. J. W. Goodman, *Introduction to Fourier Optics* (Freeman, 2017).
19. U. Leonhardt, *Science* **312**, 1777–1780 (2006).
20. J. B. Pendry, D. Schurig, D. R. Smith, *Science* **312**, 1780–1782 (2006).
21. V. M. Shalaev, *Science* **322**, 384–386 (2008).
22. See supplementary materials.
23. F. Dyson, *Nature* **427**, 297 (2004).
24. A. de Saint-Exupéry, *Le Petit Prince* (Gallimard, 1945); illustrations by the author.
25. M. Berry *et al.*, *J. Opt.* **21**, 053002 (2019).
26. S. M. Anlage, V. V. Talanov, A. R. Schwartz, *Principles of Near-Field Microwave Microscopy* (Springer, 2007).
27. K. Y. Bliokh, F. J. Rodríguez-Fortuño, F. Nori, A. V. Zayats, *Nat. Photonics* **9**, 796–808 (2015).
28. P. Cheben, R. Halir, J. H. Schmid, H. A. Atwater, D. R. Smith, *Nature* **560**, 565–572 (2018).
29. I. Liberal, N. Engheta, *Science* **358**, 1540–1541 (2017).
30. M. Kadic, T. Bückmann, R. Schittny, M. Wegener, *Rep. Prog. Phys.* **76**, 126501 (2013).

ACKNOWLEDGMENTS

We thank C. Benea-Chelmus, P. Chevalier, D. Kazakov, N. Rubin, and Z. Shi (Harvard University), as well as S. J. Klein and S. Schwettmann (MIT), for helpful advice. **Funding:** Supported by Air Force Office of Scientific Research grant AFOSR FA9550-14-1-0389. **Author contributions:** V.G. conceived the concept of cascaded mode conversion and developed the theory with inputs from M.P., M.T., S.K., and F.C.; V.G., M.P., M.T., and J.L. designed the experimental devices; M.P. carried out the measurements; and V.G., M.P., M.T., and J.L. analyzed the experimental data. All authors contributed to the writing of the manuscript. **Competing interests:** A provisional patent application has been filed on the subject of this work by the President and Fellows of Harvard College. **Data and materials availability:** All data are available in the manuscript or the supplementary materials.

SUPPLEMENTARY MATERIALS

science.sciencemag.org/content/369/6502/436/suppl/DC1
Supplementary Text
Materials and Methods
Figs. S1 to S16
Movies S1 and S2
References (*31*–*36*)

8 March 2020; accepted 29 May 2020
10.1126/science.abb6406

Remote structuring of near-field landscapes

Vincent Ginis, Marco Piccardo, Michele Tamagnone, Jinsheng Lu, Min Qiu, Simon Kheifets and Federico Capasso

Science **369** (6502), 436-440.
DOI: 10.1126/science.abb6406

Sculpting the optical near field

In the generation of electromagnetic fields, light can be broken down into two components: the far field, which we generally see and is caused by propagating waves, and the near field. The near field presents the nonpropagating component of the electromagnetic field at subwavelength distance from the source of radiation. Probing the near field, however, can also provide detailed, subwavelength information about the emitting source. Ginis *et al.* present a nanophotonic-based method for controlling and manipulating the near-field landscape. This approach provides the possibility of exploiting the near-field component of light for on-chip applications that would normally require bulky optics.

Science, this issue p. 436